Adjusting the Quasi-Stiffness of an Ankle-Foot Prosthesis Improves Walking Stability during Locomotion over Compliant Terrain

Chrysostomos Karakasis, IEEE Student Member, Robert Salati and Panagiotis Artemiadis*, IEEE Senior Member

Abstract-Despite significant advances in the design of robotic lower-limb prostheses for individuals with impaired mobility, there is a need for further progress in improving the robustness, safety, and stability of these devices in a wide range of activities of daily living. Although powered prostheses have been able to adapt to different speeds, conditions, and rigid terrains, no control strategies have been proposed for addressing walking over compliant surfaces. This work proposes a continuous admittance controller that adjusts the ankle quasistiffness of a powered ankle-foot prosthesis and improves gait stability during locomotion over compliant terrain. The proposed controller is evaluated with walking experiments on an instrumented treadmill that can accurately change the walking surface stiffness. In these experiments, the proposed controller accurately changes the prosthesis ankle quasi-stiffness across a wide range of $10-20~\frac{Nm}{deg}$, while improving local dynamic stability compared to a standard phase-variable controller. The proposed controller can significantly improve the performance of lower-limb prostheses in dynamic and compliant environments frequently encountered in daily activities, resulting in improved quality of life for people with lower-limb amputation.

I. Introduction

Over 2 million Americans are currently living with amputation, primarily of the lower limbs [1]. Individuals with lower extremity amputation present an increased rate of falling, which can lead to injury, as well as trigger a fear of physical activity [2]. To restore functional mobility and minimize the risk of falling, passive, semi-active, and powered lower-limb prostheses have been developed [3, 4]. Powered prostheses stand out as they also inject net energy to the user, while being capable of adapting to different conditions and terrains [3]. Nevertheless, no control strategy has ever been proposed focusing on walking over non-rigid terrains frequently encountered in everyday life.

Research in biomechanics shows that humans increase leg stiffness as surface stiffness decreases [5,6]. Adjusting leg stiffness has also enabled a 3-D bipedal model to achieve dynamic walking with robustness to extremely low ground-stiffness perturbations [7]. Human leg stiffness depends primarily on the torque-angle relationship or *quasi-stiffness* of the ankle [8,9]. Similarly to leg stiffness, humans increase

*This material is based upon work supported by the National Science Foundation under Grants No. #2020009, #2015786, #2025797, and #2018905. This scientific paper is partially supported by the Onassis Foundation - Scholarship ID: F ZQ029-1/2020-2021.

Chrysostomos Karakasis, Robert Salati and Panagiotis Artemiadis are with the Mechanical Engineering Department, at the University of Delaware, Newark, DE 19716, USA. chryskar@udel.edu, rsalati@udel.edu, partem@udel.edu

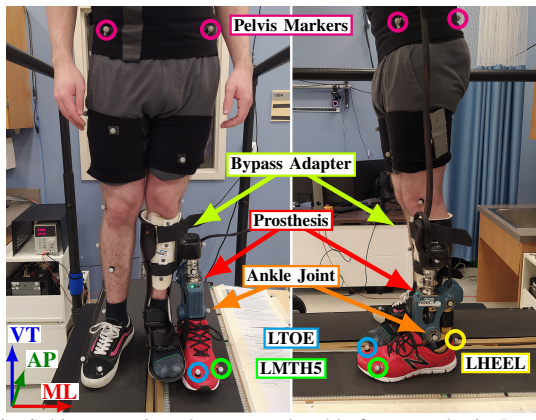


Fig. 1: Subject wearing the powered ankle-foot prosthesis Ruggedized Odyssey Ankle (ROA) through a bypass adapter, while standing on the Variable Stiffness Treadmill (VST). Magenta circles highlight the four markers around the pelvis, while blue, green, and yellow circles indicate the markers placed on the toe (LTOE), the metatarsal head #5 (LMTH5), and the heel (LHEEL) of the left prosthetic foot, respectively. Red, green, and blue axes represent the Mediolateral (ML), Anteroposterior (AP), and Vertical (VT) directions, respectively.

ankle stiffness and quasi-stiffness when surface stiffness decreases during walking or hopping [5, 10]. Therefore, previous research in legged locomotion motivates the exploitation of ankle stiffness and quasi-stiffness adjustments to support locomotion over compliant terrains.

Although some semi-active prosthetic devices allow the adjustment of their stiffness [4, 11], most ankle prostheses do not have that capability. Moreover, only fully powered prostheses can accurately mimic the functionality of the biological ankle, by providing positive net work during the gait cycle [11]. Current state-of-the-art controllers for powered prostheses include discrete impedance and continuous phasevariable controllers [3, 12, 13]. Impedance controllers exhibit increased robustness to disturbances but require switching between different modes and heuristic tuning. On the other hand, continuous controllers can seamlessly adapt to temporal changes in gait without any switching and require less tuning time. State-of-the-art controllers can adapt to different conditions, speeds, and terrains, such as uneven and ramped surfaces, as well as stairs [3, 12, 14, 15]. Among them, an impedance-based controller achieved human-like biomechanics across speeds with a powered transfemoral prosthesis by modulating ankle and knee quasi-stiffness to match intact-leg profiles [15]. However, to our knowledge, no controller has ever been designed for or evaluated over compliant surfaces. As a result, there is a need for a controller enabling robust and stable locomotion over non-rigid terrains.

^{*}Corrresponding author: partem@udel.edu

When designing and evaluating controllers for dynamic surfaces, the use of specific metrics for gait stability is essential. Several measures have been proposed in the literature for evaluating gait stability [16]. Among them, the maximum Lyapunov exponents stand out due to their validity and broad applicability across tasks and subjects, including people with lower-limb amputation [16,17]. Additionally, maximum Lyapunov exponents have correctly described increased instability during perturbed walking while differentiating overground walking from walking over compliant terrain [18]. Another stability measure that has captured the instability induced by walking over compliant terrains is the margins of stability, which are directly associated with the probability of falling due to their sound mechanical basis [16, 19, 20]. Therefore, maximum Lyapunov exponents and margins of stability seem promising candidates for evaluating gait stability over compliant terrains.

This work proposes a continuous controller that adjusts the ankle quasi-stiffness of a powered ankle-foot prosthesis and improves gait stability during locomotion over compliant terrain. First, the proposed controller enables the accurate modulation of the ankle quasi-stiffness in the employed powered prosthesis. The proposed controller is evaluated with walking experiments on an instrumented treadmill that can accurately change the walking surface stiffness. In these experiments, the proposed controller accurately changes the prosthesis ankle quasi-stiffness across a wide range of $10\, 20 \frac{Nm}{deg}$, while improving local dynamic stability compared to the standard controller. To our knowledge, this is the first time where controllers for powered prostheses are evaluated during locomotion over compliant terrain. In summary, this paper shows that stable locomotion over compliant surfaces can be achieved using the proposed controller for anklefoot prosthetic devices. This work could advance the field of lower-limb rehabilitation by improving the walking stability of people with lower-limb amputation in everyday activities, where non-rigid terrains are frequently encountered.

II. METHODS

A central feature of this paper is the introduction of a novel admittance controller for a powered ankle-foot prosthesis, followed by its comprehensive evaluation and comparison to a standard controller during locomotion over compliant terrain. First, the utilized powered ankle-foot prosthesis and its standard tibia controller are briefly analyzed in Subsections II-A and II-B, respectively. Then, the proposed admittance controller is presented in Subsection II-C, while the experimental protocol followed for the evaluation of the controllers in walking trials over compliant terrain is described in Subsection II-D. Finally, the measures utilized to evaluate gait stability are detailed in Subsection II-E.

A. Description of the Ruggedized Odyssey Ankle Prosthesis

The Ruggedized Odyssey Ankle (ROA) prosthesis, shown in Fig. 1, is a single rotational degree of freedom powered ankle-foot prosthesis developed by SpringActive, Inc. [21]. Throughout the gait cycle, energy is stored in a $377~\frac{kN}{m}$

spring, while a $250\ W$ brushless DC motor adds additional energy to the system. The motor position and ankle angle are measured by a motor and an ankle encoder, respectively. Ankle moment is defined as the moment applied by the spring about the ankle joint, and it is calculated based on motor position and ankle angle through a lookup table (LUT) created by the prosthesis manufacturer.

B. Tibia Controller

The tibia controller (TC) is a continuous phase-variable controller specifically designed for the ROA prosthesis [13]. In short, the TC utilizes the tibia kinematics to create a desired motor trajectory to replicate ankle angle trajectories of healthy non-disabled human gait. In particular, phase plane invariants of the tibia angle determine the gait percent and stride length, which are then mapped to a reference ankle angle using motion capture data from healthy non-disabled humans. In turn, a corresponding motor position (x_{tc}) is calculated based on the prosthesis dynamics, yielding a continuous reference motor trajectory throughout the gait cycle. The tibia controller has been successfully tested by people with transtibial amputation during walking and running over rigid terrain [13,21]. However, to our knowledge, the TC has not been evaluated during locomotion over compliant terrain.

C. Admittance Controller

Previous research in legged locomotion motivates the adjustment of leg stiffness to achieve locomotion over compliant terrains [5–7,10]. Specifically, significant increases in ankle stiffness and quasi-stiffness have been observed during human walking and hopping over compliant surfaces [5,10]. Inspired by this, we propose an admittance controller (AC) that adjusts the ankle quasi-stiffness of the ROA prosthesis to achieve locomotion over complaint terrain.

The proposed admittance controller is based on the TC controller analyzed in Subsection II-B, extended to allow for the adjustment of the ankle quasi-stiffness when needed. In detail, the admittance controller imposes a virtual rotary spring behavior on the single degree of freedom ankle joint:

$$M = K_d(q_d - q_e), (1)$$

where M is the externally applied moment, K_d is the stiffness of the admittance controller, and q_d, q_e are the desired and equilibrium ankle angles, respectively. As we are interested in controlling the quasi-stiffness of the ankle joint, the following feedback control law is used:

$$q_d = q_e + \frac{M}{K_d}. (2)$$

As a result, the ankle quasi-stiffness is controlled by setting the desired stiffness K_d of the admittance controller in (2).

A block diagram illustrating the implementation of the proposed admittance controller to the ankle prosthesis is shown in Fig. 2. First, the desired stiffness K_d is selected by the user and the externally applied moment M is estimated as the ankle moment calculated by the prosthesis. As mentioned in Subsection II-A, the ankle moment is computed based

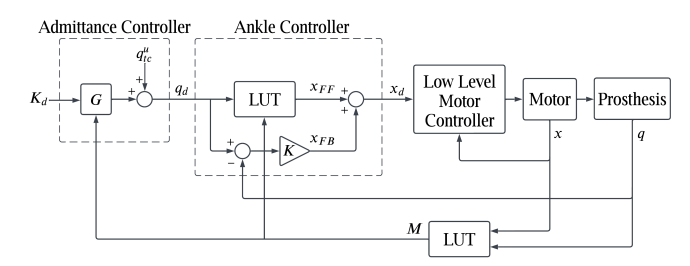


Fig. 2: Block diagram illustrating the implementation of the proposed admittance controller (AC).

on the motor position x and the ankle angle q using a LUT. Next, K_d and M are fed to the transfer function $G = \frac{M}{K_d}$ which yields an ankle angle offset. The calculated ankle angle offset is then added to the virtual unloaded reference ankle angle q^u_{tc} of the tibia controller to derive the desired ankle angle q^u_{tc} is derived by using an inverted version of the ankle moment LUT, as a function of the TC reference motor position x_{tc} and a virtual zero ankle moment. This allows the decoupling of the admittance controller from the inherent stiffness of the prosthesis, imposed by its dynamics. In summary, the proposed admittance controller receives a desired stiffness command K_d and outputs a desired ankle angle q_d to model the desired quasi-stiffness.

The desired ankle angle output from the admittance controller is next converted to a motor position command through a two-component controller (Ankle Controller). The first component is a feedforward system that determines a desired motor position x_{FF} based on the desired ankle angle and the applied ankle moment through a LUT. The second component of the controller is a proportional feedback controller with a gain K=0.45 designed to reduce errors between the desired and the actual ankle angle. The feedback controller returns a second motor position command x_{FB} , which is added to the feedforward one to derive the final desired motor position x_d sent to the low level motor controller. Finally, the low level motor controller is a feedback controller designed by SpringActive to ensure precise motor position tracking, which has been optimally tuned for the speeds and loads expected for the ROA device.

D. Experimental Protocol

For this study, a healthy non-disabled human subject (male, age: 22, height: $1.62\ m$, weight: $56.7\ kg$) tested the prosthetic device. A carbon fiber ankle bypass adapter was fitted around the left shank of the subject to allow walking with the prosthesis, whilst maintaining knee movement (Fig. 1). A heel lift was also worn in the right shoe to balance the height difference introduced by the bypass adapter.

Walking trials were performed on a unique robotic device, the Variable Stiffness Treadmill (VST) [22, 23]. The VST has been used in numerous of our studies for understanding the human gait on compliant terrain [24]. In short, the VST is a split-belt treadmill that can induce repeatable unilateral stiffness perturbations to the user walking on it, by dynamically decreasing the vertical ground stiffness of the left belt. Before any trials, the subject was instructed to

walk for several gait cycles over rigid terrain $(1 \, \frac{MN}{m})$ to get familiar with the VST and the prosthesis, as well as to find a comfortable self-selected walking speed.

In our experiment, the subject completed four walking trials at a self-selected speed of $0.6 \frac{m}{s}$. In the first trial, the standard tibia controller (TC) was utilized, while in the next three trials, the proposed admittance controller (AC) was employed with three different desired stiffness levels. For all trials, the subject experienced consecutive one-step unilateral stiffness perturbations of $30 \frac{kN}{m}$ on the left leg (prosthesis side) for 200 gait cycles. During the perturbations, the left belt of the VST emulates a surface similar to a foam pad [7], while the right side is kept rigid. In order to minimize fatigue, the subject was allowed to rest for ten minutes between trials. For safety purposes, a body weight support harness was worn by the subject around his torso, while the treadmill is also equipped with handrails for additional safety (Fig. 1). Informed consent was given, and the experimental protocol is approved by the University of Delaware Institutional Review Board (IRB ID#: 1520622-2). A supplemental video of the trials is available for download.

Kinematic data were collected using an 8-camera Vicon motion capture system at 100~Hz (Vicon Motion Systems Ltd.). The 3-D positions of 22 reflective markers placed on the subject's lower body were recorded along the Mediolateral (ML), Anteroposterior (AP), and the Vertical (VT) direction (Fig. 1). For this work, we are focusing only on the markers placed on the metatarsal head #5 (LMTH5), the toe (LTOE), and the heel (LHEEL) of the left prosthetic foot, as well as the four markers around the pelvis (Fig. 1). Prosthesis data including ankle angle and moment were also collected at 100~Hz. For all trials, the initial 25 out of the total 200 recorded strides were discarded as transient artifacts.

E. Stability Measures

In this section, the measures utilized for evaluating gait stability with each controller will be analyzed. The center of mass (CoM) position was estimated using the average 3-D position of the four pelvis markers, i.e., the left and right anterior and posterior superior iliac spine markers shown in Fig. 1. The 3-D CoM velocity was computed as the derivative of the CoM position with respect to time.

1) Maximum Lyapunov Exponent: The maximum Lyapunov or divergence exponents represent the sensitivity of a system to small perturbations by quantifying the exponential rate of divergence between neighboring trajectories in state space [25]. Specifically, larger exponents indicate greater sensitivity to local perturbations, and hence higher divergence and lower local dynamic stability. As in previous works, the maximum Lyapunov exponents were used to characterize the local dynamic stability of human walking [16].

For their calculation, Rosenstein's algorithm was used [25]. From the estimated CoM raw (unfiltered) 3-D position, the pelvis velocities were derived along the ML, AP, and VT directions (Fig. 1). The velocity time series were time-normalized to a fixed number of 150 strides and a fixed number of 15000 data points per time

series or approximately 100 data points per stride. Next, a high-dimensional attractor was reconstructed from each time-normalized velocity and its delayed copies using the method of delay embedding. The time delay and embedding dimension were individually calculated for each time series using the Average Mutual Information (AMI) algorithm and the False Nearest Neighbor (FNN) algorithm. Across all trials, time delays and embedding dimensions were on average 10 samples and $3.86\pm0.35,$ respectively, for the ML velocity, 6.47 ± 0.89 samples and 4 for the AP velocity, and 7.88 ± 0.78 samples and 4 for the VT velocity.

For each point in the reconstructed state space, the nearest neighbor j was identified, and the Euclidean distance between them was tracked for a time interval of 10 strides, resulting in a time-distance curve $d_i(i)$, where i represents discrete time instances. A divergence curve, expressed as $< \ln\{d_i(i)\} > \text{was derived as the mean of the natural}$ logarithms of the time-distance curves across all neighbor pairs j. Similar to other studies, short-term (λ_S) and longterm (λ_L) Lyapunov exponents were computed as the slopes of least-square fits applied to each divergence curve over the intervals of 0-1 strides and 4-10 strides, respectively. The average stride duration across all trials was $1.46 \pm 0.06 \ s$. To capture within-subject variability, divergence exponents were calculated for 25 overlapping segments of 150 strides (total of 175 strides) for each trial and mean values and standard deviations were computed for each exponent.

2) Margins of Stability: Suggested as a measure of stability, the margins of stability (MOS) represent the distance between the extrapolated CoM (XcoM) and the base of support (BoS) [19]. Larger positive MOS values indicate increased stability, as during unstable walking and falling the CoM approaches and exceeds the BoS. Adopting the definition from [19], XcoM was calculated as

$$XcoM = p + \frac{\dot{p}}{\omega_o},\tag{3}$$

where p and \dot{p} are the 3-D position and velocity of the CoM, respectively, and $\omega_o = \sqrt{\frac{g}{l}}$ is the eigenfrequency of a hanging non-inverted pendulum of length l, while $q = 9.81 \frac{m}{c^2}$ is the gravity acceleration. The length l was calculated as the average Euclidean distance between the LHEEL marker and the CoM at heel-strike $(l = 0.91 \pm 0.01 \ m)$. The heelstrike events were identified in real-time using the kinematic algorithm F-VESPA [26]. Although the margins of stability can be computed for both sides, we decided to focus only on the prosthesis left side that was perturbed. For every step, mediolateral margins of stability (MOS_{ML}) were calculated as the minimum medial-lateral distance between the XcoM and the lateral BoS, defined by the LMTH5 marker. Anteriorposterior margins of stability (MOS_{AP}) were computed as the maximum anterior-posterior distance during each step between the XcoM and the anterior BoS, defined by the LTOE marker. Kinematic data were filtered via a 4^{th} order, low-pass Butterworth filter (cut-off frequency of 5 Hz). For each trial, mean values and standard deviations for each MOS were calculated across a total of 175 steps.

III. RESULTS

In this section, the admittance and tibia controllers are evaluated during locomotion over a compliant terrain in four trials. The first trial evaluated the tibia controller on the compliant terrain. In the next three trials, the admittance controller was tested using the following desired stiffness K_d values: 10, 15, and 20 $\frac{N_m}{deg}$. First, the ankle quasistiffness tracking of the admittance controller is validated over the compliant terrain. Then, the performance of the two controllers is assessed and compared using two stability measures. All post-processing was implemented and executed in MATLABTM version 9.7 (R2019b) (The MathWorks, Natick, MA USA). Data were statistically tested to determine significance using the Wilcoxon rank-sum test (non-parametric counterpart to the t-test) with an α value of 0.01.

A. Ankle Quasi-stiffness Tracking of Admittance Controller

The quasi-stiffness tracking of the admittance controller was evaluated during locomotion over compliant terrain for three desired stiffness K_d levels: 10, 15 and 20 $\frac{Nm}{deg}$. Similarly to previous works, the ankle quasi-stiffness was defined as the slope of the ankle joint moment-angle curve [9, 10]. Ankle quasi-stiffness was calculated at mid-stance (60% of stance phase), where the stance phase was defined as the first 65% of the gait cycle starting from the heel-strike. The prosthesis ankle angle and moment were acquired from the prosthesis sensors at 100 Hz rate and they were filtered via a 2nd order, low-pass Butterworth filter (cut-off frequency of 5 Hz). For each trial, the average values and standard deviations of the ankle quasi-stiffness were calculated across a total of 175 steps (Table I). Furthermore, for each trial the average moment-angle curve was obtained by deriving the average ankle angle and average ankle moment profiles across a total of 175 steps (Fig. 3). For comparison purposes, the same process was applied for the trial with the TC, where the ankle quasi-stiffness was not controlled.

As shown in Fig. 3, as the desired stiffness of the admittance controller increases, the instantaneous slope of the moment-angle curve increases, hence indicating an increased ankle quasi-stiffness. This is also verified by the fact that for the same load (moment), lower angular deflection is observed for a higher desired stiffness of the admittance controller. According to these, the ankle joint appears to be significantly more compliant with the tibia controller than with all versions of the admittance controller. All of the above observations are confirmed by the calculated values of the ankle quasi-stiffness at mid-stance shown in Table I. In detail, accurate quasi-stiffness tracking is observed across the wide range of $10 - 20 \frac{Nm}{deg}$. As a result, the admittance controller in a set 11 of 12. controller is capable of significantly increasing the ankle quasi-stiffness of the prosthesis up to approximately four times the stiffness observed with the tibia controller.

B. Evaluation of the Tibia and Admittance Controllers

The proposed admittance controller was evaluated and compared to the standard tibia controller for walking over

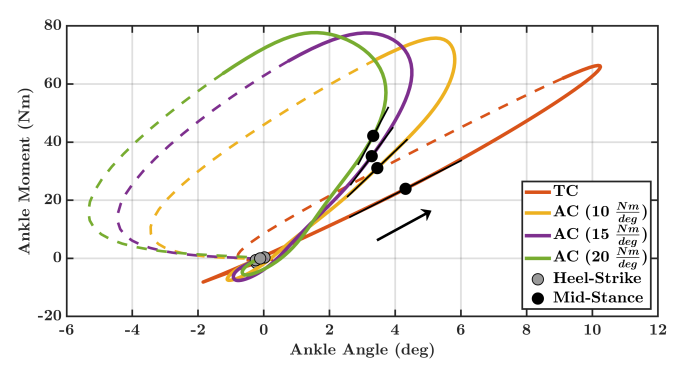


Fig. 3: Moment-angle curves of the powered prosthesis ankle joint during locomotion over compliant terrain. Orange lines correspond to the tibia controller (TC) over compliant terrain (30 $\frac{kN}{m}$), while yellow, purple, and green lines denote the admittance controller (AC) over compliant terrain with desired stiffness values of $K_d=10$, 15 and 20 $\frac{Nm}{deg}$, respectively. The black arrow indicates the increasing direction of the gait cycle (GC). Solid and dashed lines represent the stance phase (0-65% GC) and the swing phase (65-100% GC), respectively. Black and grey circles (o) indicate the time instances of mid-stance and heel-strike, respectively. Mid-stance is defined as 60% of the stance phase. The quasi-stiffness was calculated as the slope of each moment-angle curve at mid-stance (thin tangent black lines). A positive ankle angle corresponds to dorsiflexion.

Controller	Desired Stiffness (K_d) $\left[\frac{Nm}{deg}\right]$	Quasi-stiffness $\left[\frac{Nm}{deg}\right]$
TC	-	5.75 ± 0.12
AC	10	10.1 ± 0.75
AC	15	15.3 ± 1.27
AC	20	21.4 ± 2.57

TABLE I: Average ankle quasi-stiffness values of the powered prosthesis derived at mid-stance during locomotion over compliant terrain. TC and AC denote the tibia and the admittance controllers, respectively.

compliant terrain. For the evaluation, the maximum Lyapunov exponents and the MOS were used (Subsection II-E). The results are presented in Fig. 4, where mean and standard deviation values are shown for each controller.

As shown in the top part of Fig. 4a, the admittance controller exhibited significantly lower λ_S values than the tibia controller for all three CoM velocity signals (Mediolateral, Anteroposterior, and Vertical) for a quasi-stiffness of 15 $\frac{Nm}{deq}$ (p < 0.003). As larger λ_S values are associated with more unstable behavior, this indicates improved walking stability with the proposed admittance controller. For the ML CoM velocity signals, the admittance controller achieved significantly lower λ_S values than the tibia controller for a quasi-stiffness value of 20 $\frac{Nm}{deg}$ (p < 0.001), while no significant difference was observed for a quasi-stiffness of 10 $\frac{Nm}{deg}$ (p > 0.01). In the AP direction, the λ_S values of the admittance controller were significantly greater than the tibia controller for ankle quasi-stiffness values of 10 and $20 \ \frac{Nm}{deg}$ (p < 0.001). In the VT direction, the λ_S values of the admittance controller were significantly lower and greater than the tibia controller for ankle quasi-stiffness values of 10 and $20 \frac{Nm}{deq}$, respectively (p < 0.002).

As illustrated in the bottom part of Fig. 4a, the admittance controller achieved significantly lower λ_L values than the tibia controller for the VT CoM velocity signals for all three ankle quasi-stiffness values (p < 0.001). Similarly to λ_S , lower λ_L values also indicate improved walking stability. In the ML direction, the admittance controller presented

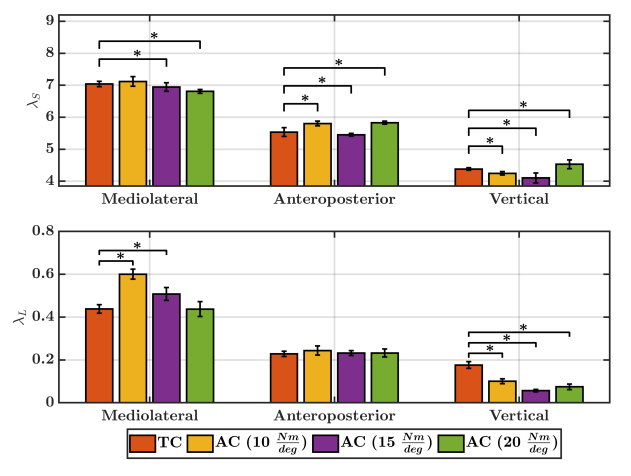
significantly greater λ_L values than the tibia controller for ankle quasi-stiffness values of 10 and 15 $\frac{Nm}{deg}$ (p < 0.001), while no significant difference was found for a quasi-stiffness of 20 $\frac{Nm}{deg}$ (p > 0.01). The λ_L values in the AP direction did not show significant differences between the tibia and the admittance controller for any of the three ankle quasi-stiffness values (p > 0.01).

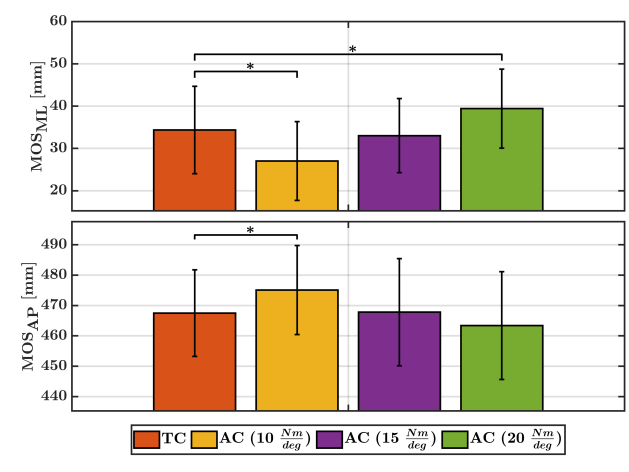
Figure 4b shows no significant difference between the tibia and the admittance controller for a quasi-stiffness of $15~\frac{Nm}{deg}$ for both margins of stability (p>0.01). For ankle quasi-stiffness values of 10 and $20~\frac{Nm}{deg},$ the admittance controller exhibited significantly lower and greater MOS_{ML} values than the tibia controller, respectively (p<0.001). In the AP direction, the admittance controller led to a significantly larger MOS than the tibia controller for a quasi-stiffness of $10~\frac{Nm}{deg}~(p<0.001),$ while no significant difference was seen for a quasi-stiffness of $20~\frac{Nm}{deg}~(p>0.01).$

In summary, short-term maximum Lyapunov exponents (λ_S) indicate a significantly improved stability across all three directions for the admittance controller with an ankle quasi-stiffness of $15 \ \frac{Nm}{deq}$. Although the long-term maximum Lyapunov exponents (λ_L) also support this finding in the VT direction, similar or worse performance is suggested in the ML and the AP direction. On the other hand, for the same directions, the margins of stability indicate similar levels of stability between the tibia and the admittance controller for the same ankle quasi-stiffness value. Therefore, these results validate that the admittance controller with an ankle quasistiffness of 15 $\frac{Nm}{deq}$ significantly improves walking stability in the VT direction compared to the standard tibia controller, without deteriorating stability in the other two directions. The fact that the admittance controller with an ankle quasistiffness of $15~\frac{Nm}{deg}$ outperforms the other controllers provides evidence that the desired ankle quasi-stiffness should be a function of the walking surface stiffness to improve stability. This agrees with our previous model-based analysis addressing bipedal locomotion over compliant surfaces [7], as well as with previous research in biomechanics studying the behavior of leg stiffness over compliant terrain [5,6,10].

IV. CONCLUSION

This paper presents a novel controller for the adjustment of the ankle quasi-stiffness in powered lower-limb prosthetic devices. The proposed admittance controller was evaluated in treadmill walking experiments with a healthy non-disabled human subject over compliant terrain. The proposed controller exhibited accurate quasi-stiffness tracking across the wide range of $10-20 \ \frac{Nm}{deg}$, whilst significantly improving local dynamic stability compared to a standard controller. As achieving stable locomotion over compliant surfaces is a critical milestone for robotic leg prostheses, this work can significantly advance the field of lower-limb rehabilitation by improving the walking stability of people with lower-limb amputations in everyday life, where non-rigid terrains are frequently encountered.





(a) Short-term λ_S (top) and long-term λ_L (bottom) maximum Lyapunov exponents. (b) Mediolateral MOS_{ML} (top) and anteroposterior MOS_{AP} (bottom) margins of stability.

Fig. 4: Stability measures. Orange bars correspond to the tibia controller (TC) over compliant terrain (30 $\frac{kN}{m}$), while yellow, purple, and green bars denote the admittance controller (AC) over compliant terrain with ankle quasi-stiffness values of 10, 15 and 20 $\frac{Nm}{deg}$, respectively. Lower λ_S - λ_L values and higher MOS_{ML}-MOS_{AP} values suggest a more stable behavior. Maximum Lyapunov exponents are expressed as ($\langle \ln\{d_j(i)\} \rangle$ /stride). Asterisks indicate significant differences between controllers (*p < 0.01).

REFERENCES

- [1] K. Ziegler-Graham, E. J. MacKenzie, P. L. Ephraim, T. G. Travison, and R. Brookmeyer, "Estimating the prevalence of limb loss in the united states: 2005 to 2050," *Archives of physical medicine and rehabilitation*, vol. 89, no. 3, pp. 422–429, 2008.
- [2] W. C. Miller, M. Speechley, and B. Deathe, "The prevalence and risk factors of falling and fear of falling among lower extremity amputees," *Archives of physical medicine and rehabilitation*, vol. 82, no. 8, pp. 1031–1037, 2001.
- [3] R. Gehlhar, M. Tucker, A. J. Young, and A. D. Ames, "A review of current state-of-the-art control methods for lower-limb powered prostheses," *Annual Reviews in Control*, vol. 55, pp. 142–164, 2023. [Online]. Available: https://www.sciencedirect.com/science/article/pii/ S136757882300007X
- [4] E. M. Glanzer and P. G. Adamczyk, "Design and validation of a semiactive variable stiffness foot prosthesis," *IEEE Transactions on Neural Systems and Rehabilitation Engineering*, vol. 26, no. 12, pp. 2351– 2359, 2018.
- [5] C. T. Farley, H. H. Houdijk, C. Van Strien, and M. Louie, "Mechanism of leg stiffness adjustment for hopping on surfaces of different stiffnesses," *Journal of applied physiology*, vol. 85, no. 3, pp. 1044– 1055, 1998.
- [6] D. P. Ferris, M. Louie, and C. T. Farley, "Running in the real world: adjusting leg stiffness for different surfaces," *Proceedings of the Royal Society of London. Series B: Biological Sciences*, vol. 265, no. 1400, pp. 989–994, 1998.
- [7] C. Karakasis, I. Poulakakis, and P. Artemiadis, "Robust dynamic walking for a 3d dual-slip model under one-step unilateral stiffness perturbations: Towards bipedal locomotion over compliant terrain," in 2022 30th Mediterranean Conference on Control and Automation (MED). IEEE, 2022, pp. 969–975.
- [8] C. T. Farley and D. C. Morgenroth, "Leg stiffness primarily depends on ankle stiffness during human hopping," *Journal of biomechanics*, vol. 32, no. 3, pp. 267–273, 1999.
- [9] E. J. Rouse, R. D. Gregg, L. J. Hargrove, and J. W. Sensinger, "The difference between stiffness and quasi-stiffness in the context of biomechanical modeling," *IEEE Transactions on Biomedical Engi*neering, vol. 60, no. 2, pp. 562–568, 2012.
- [10] K. Xie, Y. Lyu, X. Zhang, and R. Song, "How compliance of surfaces affects ankle moment and stiffness regulation during walking," Frontiers in Bioengineering and Biotechnology, p. 759, 2021.
- [11] M. K. Shepherd and E. J. Rouse, "The vspa foot: A quasi-passive ankle-foot prosthesis with continuously variable stiffness," *IEEE Transactions on Neural Systems and Rehabilitation Engineering*, vol. 25, no. 12, pp. 2375–2386, 2017.
- [12] A. H. Shultz and M. Goldfarb, "A unified controller for walking on even and uneven terrain with a powered ankle prosthesis," *IEEE Trans*actions on Neural Systems and Rehabilitation Engineering, vol. 26, no. 4, pp. 788–797, 2018.

- [13] M. A. Holgate, T. G. Sugar, and A. W. Bohler, "A novel control algorithm for wearable robotics using phase plane invariants," in 2009 IEEE International Conference on Robotics and Automation. IEEE, 2009, pp. 3845–3850.
- [14] T. K. Best, K. R. Embry, E. J. Rouse, and R. D. Gregg, "Phase-variable control of a powered knee-ankle prosthesis over continuously varying speeds and inclines," in 2021 IEEE/RSJ International Conference on Intelligent Robots and Systems (IROS). IEEE, 2021, pp. 6182–6189.
- [15] T. Lenzi, L. Hargrove, and J. Sensinger, "Speed-adaptation mechanism: Robotic prostheses can actively regulate joint torque," *IEEE Robotics & Automation Magazine*, vol. 21, no. 4, pp. 94–107, 2014.
- [16] S. M. Bruijn, O. Meijer, P. Beek, and J. H. van Dieen, "Assessing the stability of human locomotion: a review of current measures," *Journal* of the Royal Society Interface, vol. 10, no. 83, p. 20120999, 2013.
- [17] F. B. Rodrigues, A. O. Andrade, and M. F. Vieira, "Effects of inclined surfaces on gait variability and stability in unilateral lower limb amputees," *Medical & Biological Engineering & Computing*, vol. 57, pp. 2337–2346, 2019.
- [18] M. D. Chang, E. Sejdić, V. Wright, and T. Chau, "Measures of dynamic stability: Detecting differences between walking overground and on a compliant surface," *Human movement science*, vol. 29, no. 6, pp. 977– 986, 2010.
- [19] A. Hof, M. Gazendam, and W. Sinke, "The condition for dynamic stability," *Journal of biomechanics*, vol. 38, no. 1, pp. 1–8, 2005.
- [20] M. J. MacLellan and A. E. Patla, "Adaptations of walking pattern on a compliant surface to regulate dynamic stability," *Experimental brain research*, vol. 173, pp. 521–530, 2006.
- [21] J. Ward, K. Schroeder, D. Vehon, R. Holgate, A. Boehler, and M. Grimmer, "A rugged microprocessor controlled ankle-foot prosthesis for running," in 39th annual meeting of the american society of biomechanics (ASB). Columbus, 2015.
- [22] A. Barkan, J. Skidmore, and P. Artemiadis, "Variable stiffness tread-mill (VST): A novel tool for the investigation of gait," in 2014 IEEE International Conference on Robotics and Automation (ICRA). IEEE, 2014, pp. 2838–2843.
- [23] J. Skidmore, A. Barkan, and P. Artemiadis, "Variable stiffness tread-mill (VST): System development, characterization, and preliminary experiments," *IEEE/ASME Transactions on Mechatronics*, vol. 20, no. 4, pp. 1717–1724, 2014.
- [24] V. Chambers and P. Artemiadis, "Using robot-assisted stiffness perturbations to evoke aftereffects useful to post-stroke gait rehabilitation," Frontiers in Robotics and AI, vol. 9, 2022.
- [25] M. T. Rosenstein, J. J. Collins, and C. J. De Luca, "A practical method for calculating largest lyapunov exponents from small data sets," *Physica D: Nonlinear Phenomena*, vol. 65, no. 1-2, pp. 117– 134, 1993.
- [26] C. Karakasis and P. Artemiadis, "F-VESPA: A kinematic-based algorithm for real-time heel-strike detection during walking," in 2021 IEEE/RSJ International Conference on Intelligent Robots and Systems (IROS). IEEE, 2021, pp. 5098–5103.